

# Protection Challenges for North America's First Combined Cable/Overhead Double-Circuit 500 kV Transmission Line With Mutual Coupling

Denis Bucco, Curtis Sanden, Arturo Torres, and Edward Wong  
*Southern California Edison*

Jordan Bell, Normann Fischer, and John Thompson  
*Schweitzer Engineering Laboratories, Inc.*

© 2017 IEEE. Personal use of this material is permitted. Permission from IEEE must be obtained for all other uses, in any current or future media, including reprinting/republishing this material for advertising or promotional purposes, creating new collective works, for resale or redistribution to servers or lists, or reuse of any copyrighted component of this work in other works.

This paper was presented at the 70th Annual Conference for Protective Relay Engineers and can be accessed at: <https://doi.org/10.1109/CPRE.2017.8090045>.

For the complete history of this paper, refer to the next page.

Presented at the  
71st Annual Georgia Tech Protective Relaying Conference  
Atlanta, Georgia  
May 3–5, 2017

Previously presented at the  
70th Annual Conference for Protective Relay Engineers, April 2017

Previous revised edition released October 2016

Originally presented at the  
43rd Annual Western Protective Relay Conference, October 2016

# Protection Challenges for North America's First Combined Cable/Overhead Double-Circuit 500 kV Transmission Line With Mutual Coupling

Denis Bucco, Curtis Sanden, Arturo Torres, and Edward Wong, *Southern California Edison*  
Jordan Bell, Normann Fischer, and John Thompson, *Schweitzer Engineering Laboratories, Inc.*

**Abstract**—In order to reduce congestion and increase reliability, Southern California Edison (SCE) set forth to construct a new 500 kV transmission line. Due to right-of-way concerns, SCE needed to install a section of the new line underground, resulting in a combined cable and overhead transmission line. The finished line consists of two overhead sections separated by an underground section.

The inclusion of underground cables causes the line to draw significant charging current, resulting in severe overvoltage conditions when the line is open circuited or lightly loaded.

The protection package for this transmission line consists of distance protection complemented by a communications-assisted permissive scheme operating in parallel with a line current differential scheme. Because impedance-based fault locating would not be reliable for a line of this structure, we explored the use of a traveling-wave fault locator.

To verify the correct operation of the proposed protection and fault locating scheme, the transmission line and its surrounding power system were modeled in a real-time digital simulator.

This paper describes how to calculate line impedance and explores impedance-based and traveling-wave fault locating methods. It also discusses the protection challenges associated with operating a double-circuit transmission line as a single circuit and the challenges of a transmission line containing both overhead and underground conductors. Finally, the paper describes using real-time digital simulation to evaluate the performance of the protection system.

## I. INTRODUCTION

In December 2009, the California Public Utility Commission (CPUC) issued a Certificate of Public Convenience and Necessity to construct the Tehachapi Renewable Transmission Project Segments 4 through 11. Segments 6 through 8, between the Vincent and Mira Loma substations, are the focus of this paper. The initial plan routed the line through the City of Chino Hills and included 74 miles of overhead construction. The city fought to have the 500 kV lines of Segment 8 routed into the Chino Hills State Park; however, CPUC chose to route through the city instead.

Southern California Edison (SCE) selected their standard bulk power design package for the transmission line:

- System A – Line current differential relay.
- System B – Directional comparison blocking relay.
- System C – Phase distance hybrid permissive overreaching transfer trip (POTT) relay via a power line carrier (PLC).

In October 2011, SCE filed a Petition for Modification to modify Segment 8 due to recommendations made by the Federal Aviation Administration regarding marking and lighting on the double-circuit tower, which was approaching 195 feet in height.

In July 2012, SCE received orders from CPUC to submit cost and design details for alternative options of Segment 8 by February 2013. These alternative options involved rerouting the transmission line and/or going underground through the city for a section of the line in the existing right of way.

In December 2013, CPUC decided to route the section underground, thereby forcing the removal of the overhead structures, creating two transition stations for the switch from overhead to underground, and necessitating trenching in sections through the city. This revised scope included configuring the right of way to accommodate two 500 kV underground cables in place of the overhead lines.

For the underground section, SCE studied various cable system configurations, including gas-insulated lines, solid dielectric insulations cables, direct buried cables, cables in tunnels, and cables in streets. In the end, SCE decided to use cross linked polyethylene (XLPE) cables in concrete duct banks grounded at a single point [1].

The concrete ducts were constructed using open trench techniques; however, to minimize impact on the community and existing infrastructure, selected sections of the ducts were installed using trenchless techniques. Two transition stations, placed on both sides where the line switched from overhead to underground, were constructed. One of the stations was located in very hilly terrain, and the other was located in a constrained commercial site (Fig. 1 and Fig. 2). The stations connected to the 500 kV lines already under construction.



Fig. 1. West transition station



Fig. 2. East transition station

These transition stations were a possible location to install additional protective devices, which would have split the single transmission line into three separate lines; however,

SCE did not pursue this option due to the shortage of space within the stations.

The 3.98 miles of underground cables created a high-voltage issue when the transmission line was open circuited or lightly loaded, requiring reactive compensation. Because of the underground section, a PLC was no longer a suitable medium for a communications channel. SCE modified the protection package to include an IEEE C37.94 channel for the phase distance POTT scheme. Due to cost and scheduling considerations, SCE decided to retain the existing protection systems.

## II. LINE CONSTRUCTION

### A. Overall Construction

The composition of the transmission line is approximately as follows: 33 miles of a single-circuit overhead line sharing a common tower structure with a 230 kV line, 28 miles of a split-phase double-circuit overhead line operated as a single circuit, 4 miles of split-phase underground cables, and 8 miles of a single-circuit overhead line on a double-circuit tower sharing a common tower structure with a future 500 kV line. Fig. 3 shows the overall line configuration, with the overhead and underground sections noted.

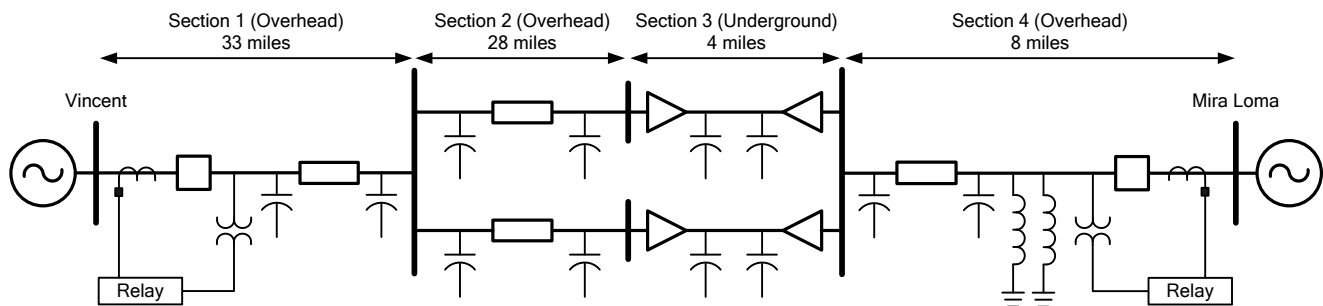


Fig. 3. Line configuration

### B. Overhead Section

The tower structure for the single-circuit and double-circuit lines is similar. For the first 33 miles, the 500 kV line (Line 1) shares a common tower structure with the 230 kV line (Line 2), as shown in Fig. 4. The proximity of these two lines leads to a strong mutual coupling between them. Furthermore, these lines are not transposed. At the 33-mile mark, the 230 kV line tees off, and the line is operated as a single-circuit line on a double-circuit structure with jumpers installed between similar phases (Fig. 5).

After 28 miles, the line configuration changes from overhead conductors to underground cables. At this stage, the line is still a single-circuit line operating on a double-circuit structure. The line continues underground for approximately 4 miles before once again becoming an overhead line for the remaining 8 miles.

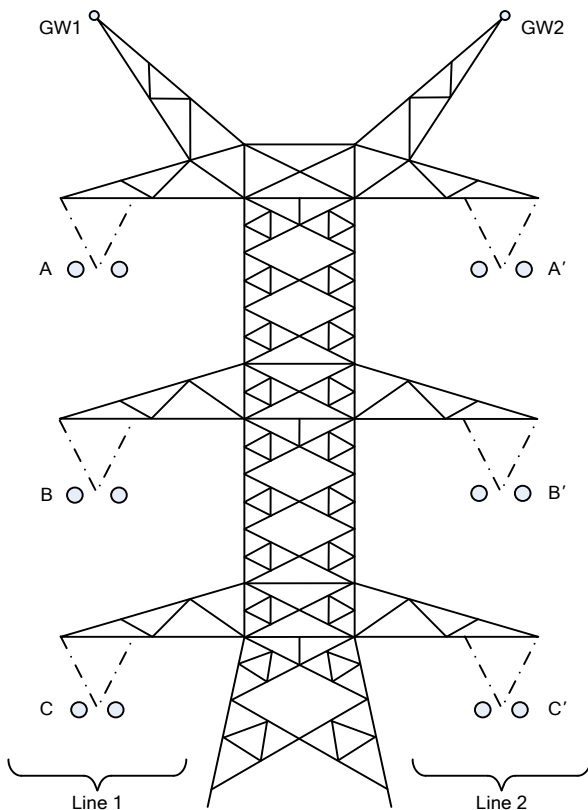


Fig. 4. Tower configuration for the 500 kV and 230 kV lines

When the transmission line is a single circuit operating on a double-circuit structure, the conductors of the same phase are only jumpered at the 33- and 68-mile marks. A single-circuit line operating on a double-circuit structure reduces both the series impedance of the line and the shunt impedance by half. In addition, a line operating in this mode draws twice as much charging current. Operating the line in this manner significantly impacts the impedance calculated by a distance relay for a fault in this section of the transmission line, which will be addressed later in this paper.

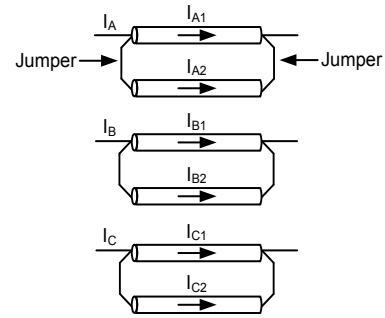


Fig. 5. Jumpered phase conductors

### C. Ground Wires

The overhead ground wires consist of one optical fiber ground wire and one steel overhead ground wire; the wires are grounded on both sides of each tower at a single point, leading to a segmentation of the ground wires (Fig. 6).

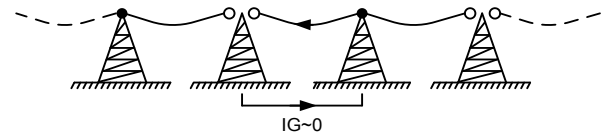


Fig. 6. Segmented ground wires

Under normal conditions, the magnitude of the phase currents and the unequal spacing of the phase conductors in relation to the ground wire induces a voltage in the ground wire. This induced voltage leads to a circulating current, which in turn leads to losses proportional to the positive-sequence current flowing through the phase conductors.

Segmenting the ground wires prevents this flow of circulating current [2]; therefore, the ground wires carry no significant current at the power system frequency (60 Hz in North America) during normal or fault conditions. For this reason, segmented ground wires can be ignored in the computation of the series impedance matrix of the line; however, the ground wires must be considered when computing the shunt impedance matrix [3].

The approximate impedances for the overhead sections of the transmission line are as follows:

- $Z_1 = 0.05 + j0.58$  ohms/mile
- $Z_0 = 0.44 + j2.13$  ohms/mile

### D. Underground Sections

The overall length of the underground cables is 3.98 miles using XLPE cables (Fig. 7). However, two underground cables located in separate ducts are used per phase (Fig. 8).

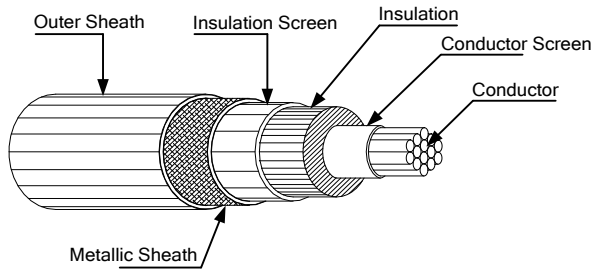


Fig. 7. XLPE cable construction

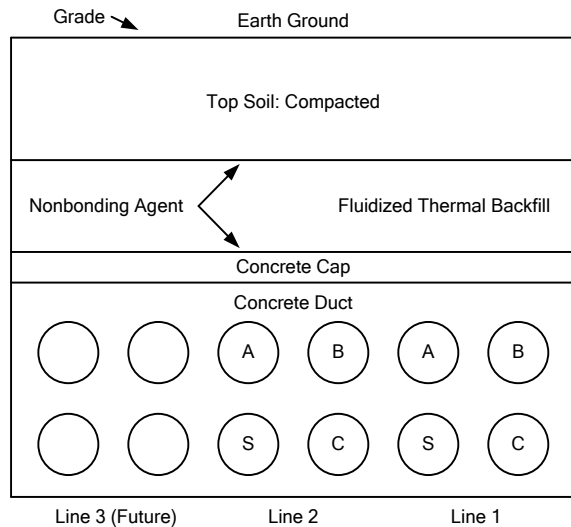


Fig. 8. Concrete duct bank

The approximate impedances for the underground sections of the transmission line are as follows:

- $Z_1 = 0.02 + j0.31$  ohms/mile
- $Z_0 = 0.20 + j0.13$  ohms/mile

The electrical characteristics of underground cables differ from overhead conductors. Underground cables have a lower series inductance and a higher shunt capacitance, leading to a zero-sequence impedance that is less than the positive-sequence impedance [1].

The series inductance of an underground cable is typically 50 percent lower than an overhead conductor due to the close spacing of adjacent conductors. The shunt capacitance of underground cables can be up to 30 to 40 times higher than overhead lines. This high capacitance is due to the cable sheath, the dielectric constant of the insulation, and the close proximity of the cable to ground potential [1].

#### E. Line Reactors for Voltage Issues

The positive-sequence charging current for a transmission line under balanced system conditions is calculated as follows:

$$I_{1\_CHRG} = j\omega C_1 \frac{V_{Ph-Ph}}{\sqrt{3}} \quad (1)$$

To calculate the charging current, we must know the positive-sequence capacitance of the line. If the length and operating voltage of the transmission line are known, then we can calculate a rough estimate of the charging current without knowing the positive-sequence capacitance. For example, a

typical 500 kV overhead transmission line draws approximately 2 amperes of charging current per mile and a 500 kV XLPE cable draws approximately 40 amperes per mile, approximately 20 times that of the overhead conductor. Therefore, the estimated charging current ( $I_{CHRG}$ ) is calculated as follows:

$$\begin{aligned} I_{CHRG} &= 33 \cdot 2 \text{ A} + (28 \cdot 2 \text{ A}) \cdot 2 + (4 \cdot 40 \text{ A}) \cdot 2 + 8 \cdot 2 \text{ A} \\ &= 514 \text{ A} \\ &\approx 467 \text{ MVAR (at 525 kV)} \end{aligned}$$

Once the line charging current is calculated, the voltage at the remote terminal under no-load conditions is calculated as follows:

$$V_{REMOTE} = V_{LOCAL} - I_{CHRG} \cdot Z_{I\_LINE} \quad (2)$$

The distributed capacitance along the line will siphon off a portion of the charging current, as illustrated in Fig. 9.

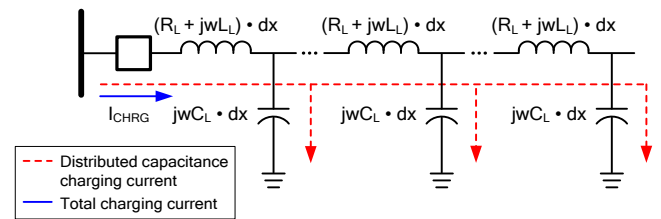


Fig. 9. Charging current drawn by the distributed capacitance

Based on the amount of charging current drawn by the overhead and underground sections (approximately 194 amperes and 320 amperes, respectively), the line energized from the Vincent substation will produce a greater voltage at the remote end. This increase in voltage is created because the majority of the charging current has to travel 60 miles to the underground section, whereas energization from the Mira Loma substation only travels 8 miles.

This amount of charging current (capacitive current) under no-load or lightly loaded conditions creates significant overvoltage. In both conditions, the baseline system voltage would be approximately 550 kV. For this reason, two 173 MVAR line reactors rated at 525 kV each were installed at the Mira Loma line end to provide approximately 70 percent shunt compensation.

Fig. 10 shows the voltage profile of the line energized from the Vincent substation, where the red line represents the uncompensated voltage and the blue line represents the compensated voltage. The open-ended voltage for the uncompensated line increased by 30 kV. In comparison, the compensated voltage barely increased by several kilovolts.

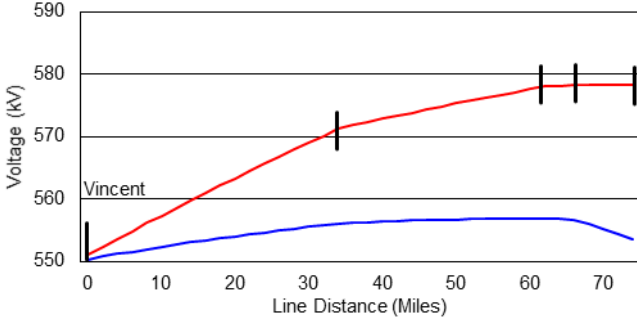


Fig. 10. Vincent voltage profile with Mira Loma open ended

Fig. 11 shows the voltage profile of the line energized from the Mira Loma substation, where the blue line represents the uncompensated voltage. Only the uncompensated voltage is shown because the open-ended voltage increased by 10 kV, showing no risk of an overvoltage condition and therefore not requiring shunt compensation.

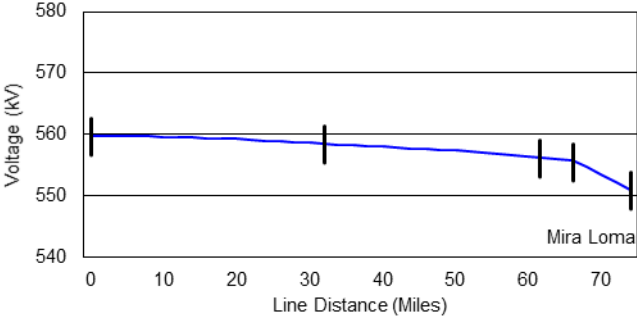


Fig. 11. Mira Loma voltage profile with Vincent open ended

From the Mira Loma substation, the majority of the charging current goes into the underground section. Energizing the remainder of the line requires only the remaining 194 amperes.

### III. LINE IMPEDANCE CALCULATION

Calculating the total line impedance for a line of this composition is not a trivial matter. For example, if we consider the voltage drop along the first section of the transmission line (the 33 miles of structure shared with the 230 kV line), we can write the following equation for the A-phase in Line 1 [4].

$$\begin{aligned} V_{A\_DROP} = & Z_{AA} \cdot IA + Z_{AB} \cdot IB + Z_{AC} \cdot IC + Z_{AA'} \cdot IA' + \\ & Z_{AB'} \cdot IB' + Z_{AC'} \cdot IC' \end{aligned} \quad (3)$$

where:

$Z_{AA}$  is the self impedance of the A-phase conductor.

$Z_{A\phi}$  is the mutual impedance between the A- and  $\phi$ -phase conductors ( $\phi = B$  and  $C$ ).

$Z_{A\phi'}$  is the mutual impedance between the A-phase conductor Line 1 and  $\phi$ -phase conductor Line 2 ( $\phi = A, B,$  and  $C$ ).

$I\phi$  is the  $\phi$ -phase current Line 1 ( $\phi = A, B,$  and  $C$ ).

$I\phi'$  is the  $\phi$ -phase current Line 2 ( $\phi = A, B,$  and  $C$ ).

We can write similar equations for the remaining phases in Lines 1 and 2 and then express those equations in matrix form as follows:

$$\begin{pmatrix} V_{A\_DROP} \\ V_{B\_DROP} \\ V_{C\_DROP} \\ V_{A'\_DROP} \\ V_{B'\_DROP} \\ V_{C'\_DROP} \end{pmatrix} = \begin{pmatrix} Z_{AA} & Z_{AB} & Z_{AC} & Z_{AA'} & Z_{AB'} & Z_{AC'} \\ Z_{BA} & Z_{BB} & Z_{BC} & Z_{BA'} & Z_{BB'} & Z_{BC'} \\ Z_{CA} & Z_{CB} & Z_{CC} & Z_{CA'} & Z_{CB'} & Z_{CC'} \\ Z_{A'A} & Z_{A'B} & Z_{A'C} & Z_{A'A'} & Z_{A'B'} & Z_{A'C'} \\ Z_{B'A} & Z_{B'B} & Z_{B'C} & Z_{B'A'} & Z_{B'B'} & Z_{B'C'} \\ Z_{C'A} & Z_{C'B} & Z_{C'C} & Z_{C'A'} & Z_{C'B'} & Z_{C'C'} \end{pmatrix} \cdot \begin{pmatrix} IA \\ IB \\ IC \\ IA' \\ IB' \\ IC' \end{pmatrix} \quad (4)$$

In (4), the impedance matrix ( $Z_{ABC}$ -matrix) contains the self and mutual impedance of the two transmission lines in the phase domain. In order to set a distance relay, we need to obtain the positive-sequence ( $Z_1$ ) and zero-sequence ( $Z_0$ ) impedances of the line. Furthermore, to correctly set the ground distance element, we need to account for the zero-sequence mutual coupling between the two transmission lines. Converting a 6x6 phase impedance matrix to the sequence domain is a straight forward process: Divide the 6x6  $Z_{ABC}$ -matrix into four 3x3 submatrices (Fig. 12).

$$\begin{pmatrix} Z_{AA} & Z_{AB} & Z_{AC} & Z_{AA'} & Z_{AB'} & Z_{AC'} \\ Z_{BA} & \mathbf{3x3} & Z_{BC} & Z_{BA'} & \mathbf{3x3} & Z_{BC'} \\ Z_{CA} & Z_{CB} & Z_{CC} & Z_{CA'} & Z_{CB'} & Z_{CC'} \\ Z_{A'A} & Z_{A'B} & Z_{A'C} & Z_{A'A'} & Z_{A'B'} & Z_{A'C'} \\ Z_{B'A} & \mathbf{3x3} & Z_{B'C} & Z_{B'A'} & \mathbf{3x3} & Z_{B'C'} \\ Z_{C'A} & Z_{C'B} & Z_{C'C} & Z_{C'A'} & Z_{C'B'} & Z_{C'C'} \end{pmatrix} = \begin{pmatrix} Z_{ABC\_I} & & & \\ & Z_{ABC\_II} & & \\ & & Z_{ABC\_III} & \\ & & & Z_{ABC\_IV} \end{pmatrix}$$

Fig. 12. 6x6  $Z_{ABC}$ -matrix divided into four 3x3 submatrices

Once this division is complete, convert each of the 3x3 submatrices ( $Z_{ABC\_I}$ ,  $Z_{ABC\_II}$ ,  $Z_{ABC\_III}$ , and  $Z_{ABC\_IV}$ ) to the sequence domain as follows:

$$Z_{012} = A^{-1} \cdot Z_{ABC} \cdot A \quad (5)$$

where:

$$A = \begin{pmatrix} 1 & 1 & 1 \\ 1 & a^2 & a \\ 1 & a & a^2 \end{pmatrix} \quad (6)$$

$$a = e^{j\frac{2\pi}{3}}$$

After each individual 3x3 submatrix has been converted to the sequence domain ( $Z_{012}$ ), we rebuild the 6x6 matrix (7) in the same order as the phase sequence shown in Fig. 12.

$$(Z_{012}) = \begin{pmatrix} Z_0 & w & x & Z_{0M} & w_m & x_m \\ w & Z_1 & y & w_m & Z_{1m} & y_m \\ x & y & Z_2 & x_m & y_m & Z_{2m} \\ Z_{0M} & w_m & x_m & Z_{0'} & x' & y' \\ w_m & Z_{1m} & y_m & x' & Z_{1'} & z' \\ x_m & y_m & z_{2m} & y' & z' & Z_{2'} \end{pmatrix} \quad (7)$$

Examining (7) yields the sequence impedances ( $Z_0$ ,  $Z_1$ , and  $Z_2$ ) of Line 1 given by the diagonal terms of the top left 3x3 submatrix. The sequence impedances ( $Z_{0'}$ ,  $Z_{1'}$ , and  $Z_{2'}$ ) of Line 2 are given by the diagonal terms of the bottom right 3x3 submatrix. The top right and bottom left 3x3 submatrices are the mutual coupling sequence components between the two

lines. Of these, the zero-sequence mutual coupling component ( $Z_{0M}$ ) is the most dominant. Because the two lines are not perfectly transposed, the off-diagonal terms of the individual 3x3 submatrices are non-zero. This means that the sequence component networks are not perfectly decoupled from one another. In our particular case, the off-diagonal terms are less than 5 percent of the value of the diagonal terms; therefore, for all practical purposes, we can ignore them. However, the zero-sequence mutual coupling ( $Z_{0M}$ ) is 55 percent of  $Z_0$  and must be considered when setting ground distance elements regardless of whether or not the lines are transposed.

For Section 2 (where the line is a double circuit operated as a single circuit), we create a similar impedance matrix as that given in (3). We then perform the transformation and obtain a sequence impedance matrix similar to the one we obtained in (7). Using this matrix, we can ascertain the sequence impedance for each of the lines as before. However, in this instance, the lines are effectively connected in parallel due to the jumpers used to operate the line as a single circuit. The effective impedance of this section of the line when viewed from the line terminals is the parallel combination of the two individual lines. Typically, the conductors used for the two lines are identical; therefore, the effective impedance when viewed from the line terminals will be half the impedance of one of the lines. We use the effective impedance (half the impedance of one of the lines) when determining the total impedance of the line, leading to the positive- and zero-sequence impedances (Equations (8) and (9), respectively):

$$Z_{1MAG} = \frac{Z_1 \cdot Z_1}{Z_1 + Z_1} \quad (8)$$

$$Z_{0MAG} = \frac{Z_0 + Z_{0M}}{2} \quad (9)$$

However, we need to be aware that if a fault occurs in this section of the line, the impedance to the fault point when viewed from the line terminals will not be  $m$  times the effective impedance [5]. For example, consider the fault at distance  $m$  from Terminal S shown in Fig. 13.

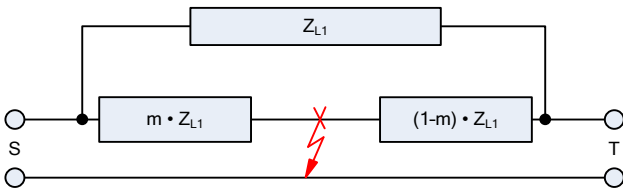


Fig. 13. Fault point at  $m$  distance

The impedance seen from Terminal S is:

$$Z_{S\_TERM} = m \cdot Z_{L1} (1 - \frac{1}{2} m) \quad (10)$$

The impedance seen from Terminal T is:

$$Z_{T\_TERM} = \frac{1}{2} \cdot Z_{L1} \cdot (1 - m^2) \quad (11)$$

Based on (10) and (11), the impedance as seen from the terminals is not a linear function of the line impedance ( $Z_{L1}$ ) and the distance to fault ( $m$ ). It is important to be aware of this nonlinearity when setting a distance element.

Section 3 of the transmission line consists of approximately 4 miles of underground cable. From the impedance point of view, we form another 6x6 matrix because the structure of this section is similar to Section 2. The effective impedance for this section is once again the parallel combination of Lines 1 and 2.

Section 4 is similar to Section 1 because this section of the line shares a common tower with the future 500 kV line.

The total impedance of the line equals the summation of the impedance of the four individual sections, as follows:

$$\left( Z_{012\_TOTAL} \right) = \left( \begin{array}{c|c} Z_{012\_I} & Z_{012\_II} \\ \hline \text{---}6 \times 6\text{---} & \\ Z_{012\_III} & Z_{012\_IV} \end{array} \right) + \left( \begin{array}{c|c} Z_{012\_I} & Z_{012\_II} \\ \hline \text{---}6 \times 6\text{---} & \\ Z_{012\_III} & Z_{012\_IV} \end{array} \right) + \left( \begin{array}{c|c} Z_{012\_I} & Z_{012\_II} \\ \hline \text{---}6 \times 6\text{---} & \\ Z_{012\_III} & Z_{012\_IV} \end{array} \right) + \left( \begin{array}{c|c} Z_{012\_I} & Z_{012\_II} \\ \hline \text{---}6 \times 6\text{---} & \\ Z_{012\_III} & Z_{012\_IV} \end{array} \right)$$

Section 1                  Section 2                  Section 3                  Section 4

The positive-sequence impedance calculated for each section is as follows:

- Section 1 = 2.01 + j19.63
- Section 2 = 0.81 + j8.19
- Section 3 = 0.04 + j0.61
- Section 4 = 0.40 + j4.89

The zero-sequence impedance calculated for each section is as follows:

- Section 1 = 11.02 + j72.70
- Section 2 = 9.63 + j50.76
- Section 3 = 0.40 + j0.25
- Section 4 = 3.69 + j18.94

Combining all four sections yields the following:

- $Z_{1MAG} = 3.26 + j33.32$  ohms
- $Z_{0MAG} = 24.73 + j142.65$  ohms

Once we determine the total impedance of the line, we can set a relay impedance element. However, we must take into account the effects of both the zero-sequence mutual coupling coefficient and the single-circuit line operating on a double-circuit structure.

#### A. Line Impedance from Energization

We modeled the transmission line in a real-time digital simulator using the geometric tower and underground construction data in order to validate the calculated line impedance. Once the transmission line was modeled appropriately, we energized it in the simulation by connecting a source to the Vincent terminal and grounding all three phases together at the remote terminal with the remote end open circuited. We then measured the sequence impedances from the applied voltages and currents.

We performed the positive-sequence test by connecting a three-phase source, which required a balanced set of three-phase voltages and currents (Fig. 14). The test yielded the  $Z_{1MAG}$  for the entire line.

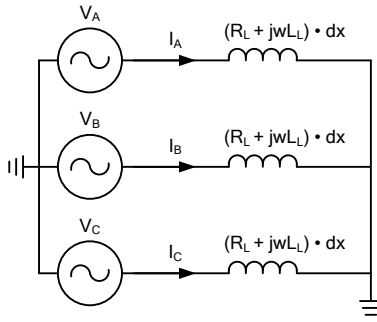


Fig. 14. Positive-sequence impedance test connection

We performed the zero-sequence test by connecting all three phases to a single source (Fig. 15). The characteristics of zero-sequence voltage and current require all three phases to be in phase with one another. This test yielded the Z0MAG for the entire line.

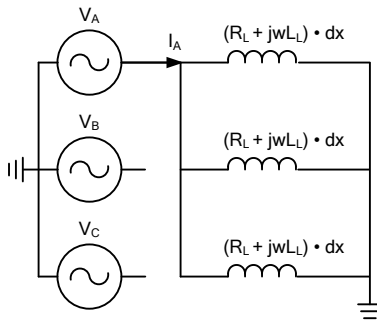


Fig. 15. Zero-sequence impedance test connection

The following impedances were measured:

- $Z_1 = 3.56 + j33.92$  ohms
- $Z_0 = 25.30 + j144.80$  ohms

We compared the value calculated using the impedance matrices against the measured values from the simulation. This comparison resulted in a positive-sequence difference of 1.9 percent and a zero-sequence difference of 1.5 percent. This difference is caused by the sequence networks not being fully decoupled.

#### IV. PROTECTION PHILOSOPHY

##### A. Overall Protection System

The transmission line uses the SCE standard bulk power protection package, which consists of three high-speed independent systems using devices produced by two manufacturers (Manufacturer A and Manufacturer B). The systems are labeled A, B, and C and consist of the following:

- System A – Line current differential relay with phase distance and directional ground functions via a digital channel (IEEE C37.94).
- System B – Hybrid POTT with directional ground comparison functions via a digital channel (IEEE C37.94).
- System C – Phase POTT and direct transfer trip (DTT) with directional ground functions via a PLC or digital channel (IEEE C37.94).

The SCE transmission lines terminating in the substations have two circuit breakers, each equipped with three sets of current transformers (CTs) on either side of the circuit breaker. Each protection system is supplied by its own CT and summed externally from each circuit breaker. Line potential transformers (PTs) with two separate secondaries are employed, and the protection is split between the two secondaries. Communication consists of two separate digital channels on diverse routes along with a single PLC channel. Two sets of DTT equipment are used to key the DTT to the remote terminals.

Because each protection system has high-speed communications-aided protection functions and backup and non-communications-aided tripping elements, all three systems are functionally equivalent. Any one system may be taken out of service for maintenance without compromising the integrity of the line protection. The failure of one communications path will only impact one protection system and one DTT system at most. In order to meet the minimum requirement of SCE to keep the majority of transmission lines in service, one primary relay system and one DTT system must be available. The choice of three primary protection systems allows most lines to remain in service even in the event of an N-2 outage.

Because the SCE transmission system is well connected with multiple ties to adjacent stations and few long lines, there are no concerns with regards to stability or losing synchronism after transmission line relay operations. As such, the relays employ three-pole tripping instead of single-pole tripping, allowing for faster fault extinguishing. Where needed, high-speed reclosing is enabled using the breaker failure protection and control relay. The relays initiate reclosing by any of the primary tripping elements. The relays will block reclosing if switch on to fault (SOTF) operates for a fault or if a three-phase fault is detected. These are generally more permanent types of faults where reclosing should be avoided.

At present, the relays on the Vincent-Mira Loma line do not perform high-speed reclosing. This avoids stressing the underground cables in the event of a fault occurring in the underground section. The configuration of the various line sections prevents the existing protection system from accurately determining whether the fault location is within the underground section. For this reason, we explored and evaluated traveling-wave (TW) fault locating methods.

SCE employs negative-sequence polarized directional ground overcurrent protection instead of ground distance protection to avoid overreach and underreach due to the extensive mutual coupling throughout the SCE transmission network. The transmission network system contains adequate ground sources to supply ground fault current through the multiple autotransformer banks located at each station.

##### B. System A: Line Current Differential Relay

System A uses a current differential protection scheme, which compares currents from a local terminal with the currents received from the remote terminal through an IEEE C37.94 digital communications channel. This

comparison is used to determine whether the fault is inside or outside of the protected zone. Phase distance and directional ground overcurrent elements were added to provide overreaching and backup protection for a loss-of-communication condition.

### C. System B: Hybrid POTT With Directional Ground Comparison

System B uses a hybrid POTT scheme with overreaching phase distance and ground directional overcurrent elements to provide high-speed tripping through an IEEE C37.94 digital communications channel. The system uses reverse looking blocking elements and echo keying. In addition, a directional comparison blocking scheme using the same IEEE C37.94 digital communications channel provides faster tripping than the hybrid POTT scheme for certain types of internal faults (e.g., an open remote breaker condition). Phase distance elements, directional ground overcurrent elements, and SOTF were added to provide overreaching and backup protection for a loss-of-communication condition.

### D. System C: Phase POTT With Directional Ground

System C provides high-speed tripping using a POTT scheme with overreaching phase distance and ground directional overcurrent elements. The original design included Frequency Shift Keying (FSK) communication over a PLC; however, SCE decided to use an IEEE C37.94 digital communications channels after the addition of the underground line section. Phase distance elements, directional ground overcurrent elements, and SOTF were added to provide overreaching and backup protection for a loss-of-communication condition.

### E. DTT Remote Breaker Tripping

The DTT protection scheme was separated into three systems: Systems A, B, and C:

- Systems A and B – The relays key a DTT for any relay trip, breaker failure operation, or open circuit breaker. Both IEEE C37.94 digital communications channels operate on diverse routes from one another.
- System C – Keying inputs on the System A protective relay for any breaker failure operation or open circuit breaker initiates a third DTT signal. The signal is sent using the System A IEEE C37.94 digital communications channel. While this method does not use separate independent DTT equipment, it provides a third independent communications channel for a DTT.

### F. Communications Channels

The three SCE standard bulk power protection systems use three independent communications channels: two separate IEEE C37.94 digital channels over diverse routes and one FSK channel over a PLC. On transmission lines where the loading exceeds 3000 amperes, SCE has discouraged using PLCs because of the size and expense of wavetraps. The option of using a PLC on the mixed overhead and underground Vincent-Mira Loma line was eliminated due to

anticipated issues with attenuation, signal-to-noise ratio problems, and reflections from the overhead and underground junctions. In place of a PLC, SCE has traditionally used a digital communications channel on one route for System A, a second digital communications channel on a diverse route for System B, and two digital communications channels that use the diverse Systems A and B routes for System C. For the Vincent-Mira Loma line, three diverse routes were provided with each protection system using one digital communications channel on diverse routes.

## V. PROTECTION SYSTEM VALIDATION

### A. Real-Time Digital Simulation

To validate the protection system, a real-time digital simulator was used to perform closed-loop testing.

The overall system short-circuit model was reduced to an equivalent network that we modeled in the transient environment. This equivalent network was comprised of 18 substations, including the entire SCE 500 kV transmission system, with equivalents at the 230 kV voltage level and in the neighboring utilities.

System planning and protection engineers collaborated to determine the following realistic system operating conditions that would challenge the protection system:

- System normal
- System weak behind each terminal
- Parallel transmission paths out of service

### B. Test Procedure

All three protection systems from both terminals were tested simultaneously and analyzed for proper operation.

Table I lists some of the typical tests performed for the 500 kV line protection system. Approximately one week was required for testing. For additional information regarding tests typically performed, refer to [6], [7], and [8].

TABLE I  
TEST PLAN

Test Number	Test Procedure
1	Basic internal/external faults
2	Line energization and load pickup
3	Zone 1 margin
4	High-impedance faults
5	SOTF
6	Evolving faults
7	Cross country faults
8	Bolted faults batch tests
9	Internal high-impedance faults batch tests

Tests 1 through 4 fine tune the normal protection elements and ensure they are properly set before running the batch tests (Tests 8 and 9). Tests 5 through 7 are used to set or understand specific protection elements or to discover the limitations of the protection devices used.

Tests 8 and 9 gather an overall picture of the performance of the protection system over various load flow cases. A typical batch test consists of the following:

- All load flow cases.
- All internal and external fault locations (21 internal and 10 external).
- Ten fault types (AG, BG, CG, ABG, BCG, CAG, AB, BC, CA, and ABCG).
- Four points on wave (0, 30, 60, and 90 degrees).

Running the batch tests resulted in more than 6000 individual faults applied to the protection system. The real-time digital simulator saves oscillographic records for each fault and stores them in Common Format for Transient Data Exchange (COMTRADE) files. The real-time digital simulator also saves space delimited text files that contain the elapsed time between fault initiation and element assertion for 90 digital signals from the output contacts of the relay that are brought into the simulation.

We developed analysis spreadsheets to facilitate processing and analyzing the generated data. The graphs include the average and maximum trip times of the relays for faults along the line as well as the coverage of the Zone 1 elements and overcurrent elements along the line.

The batch tests were run multiple times. Each time, the testing team thoroughly investigated undesired operations and poor performance cases identified by the data. In keeping with conventional practices when encountering undesired operations, we began the analysis by examining the COMTRADE record from the faults of interest. Where necessary, we repeated faults and downloaded detailed event records from the relays. After discovering root cause, we proposed and validated a solution. We then repeated the batch tests using the new settings to verify the desired performance.

### C. Test Results

#### 1) Distance Elements

We applied faults along the line in five-percent increments, starting at the Vincent substation and moving toward the Mira Loma substation. We then captured relay event records for each fault and ran them through a relay analysis file to record the mho phase loops in order to verify the measurement against the line impedance [9]. In Fig. 16 and Fig. 17, the black line represents the theoretical impedance calculation from the respective terminal, the blue line represents the Vincent relay measurements, and the red line represents the Mira Loma relay measurements. We applied bolted faults to the overhead sections. For the underground section, we only considered core-to-ground faults [1].

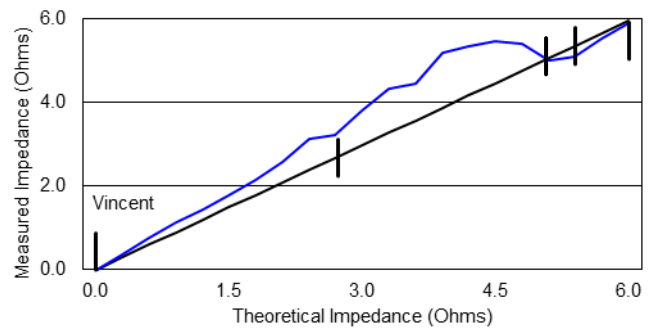


Fig. 16. Vincent terminal three-phase impedance measurement of Manufacturer A

As the fault moved away from the Vincent terminal, the non-linearity effect of the apparent impedance caused the relay to underreach. We obtained similar results for the Mira Loma terminal; however, in this case, the relay tended to overreach because the split-phase section is closer to that terminal (Fig. 17).

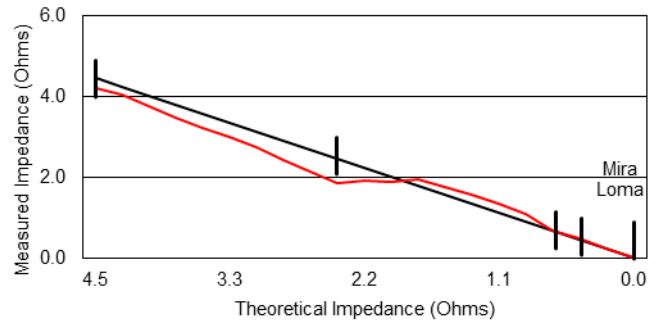


Fig. 17. Mira Loma terminal three-phase impedance measurement of Manufacturer A

The results show the non-linearity effect seen from the two terminals. If the line was split-phase for the entire length of the line, the overreaching distance elements would need to increase their reach to reliably detect internal faults. In this application, we did not adjust the overreaching distance elements because they reliably detected the internal faults.

#### a) Distance element performance with jumper removed

During testing, one of the jumpers on the split-phase sections was removed (Fig. 18).

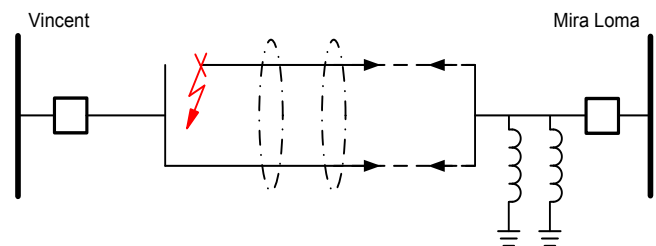


Fig. 18. Location of removed jumper

With the jumper removed, a three-phase fault was then applied (Fig. 18). We recorded the measurement of the distance element from the Vincent terminal relay, where the black line is the A-phase to B-phase mho loop, the red line is the B-phase to C-phase mho loop, and the blue line is the C-phase to A-phase mho loop (Fig. 19).

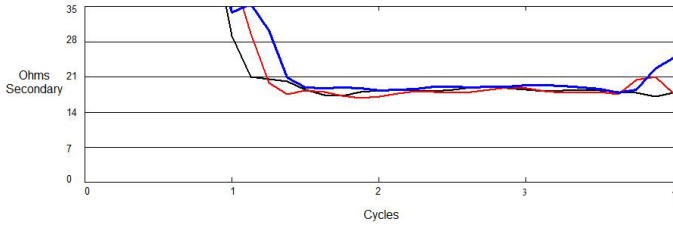


Fig. 19. Vincent terminal impedance measurement of Manufacturer A

The measured phase-to-phase mho loops were more than three times the overall line impedance, meaning that the phase distance elements would have to be set upwards of 400 percent of the line impedance to adequately detect the fault. For the Mira Loma terminal relay, the fault was still within the reach of the Zone 1 element. The test was performed to understand the impact of the split-phase section on the distance elements. No changes were made from this test because the event is extremely unlikely to occur. Furthermore, the line current differential protection and diverse DTT paths mitigate this fault scenario.

A splice failure was considered at the same location as the three-phase fault, emulating a conductor falling and hitting the ground. In this scenario, the overcurrent elements detected the fault and operated as expected.

*b) Batch tests*

Batch tests were run for faults at each location with varying point-on-wave fault inception angles and for various load flow cases. Fig. 20 shows the results of the coverage of the Zone 1 distance element along the line for the first round of Manufacturer A relay testing. For Fig. 20 through Fig. 25, blue indicates the Vincent terminal and red indicates the Mira Loma terminal. Because only phase distance elements are used, the expected number of operations is 70 percent of the faults applied; the remaining 30 percent are single-line-to-ground (SLG) faults that phase distance elements should not operate for.

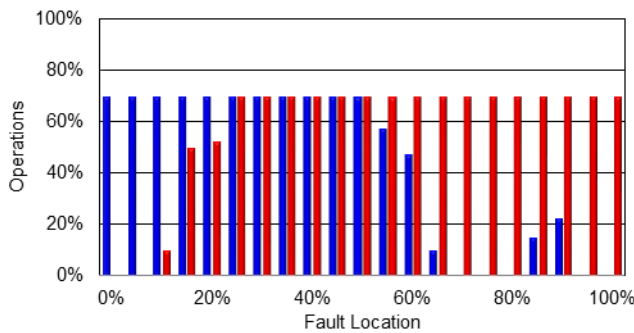


Fig. 20. Manufacturer A Zone 1 operations

The results revealed that under certain system conditions, the Zone 1 elements would transiently assert at 85 to 90 percent of the line. Given the typical SCE setting of 80 percent, this produced a greater reach than expected. Fig. 21 shows the impedance measurement from one event.

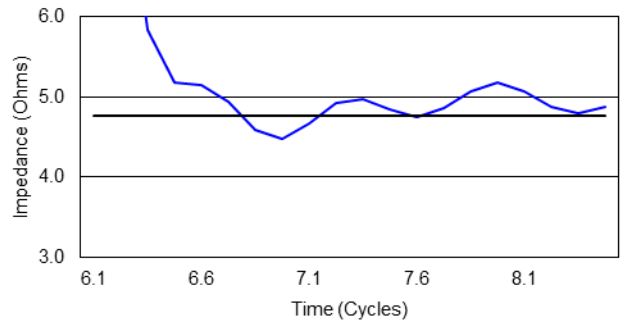


Fig. 21. Manufacturer A mho ground impedance measurement

The reach was reduced to 70 percent for all relays to maintain consistent settings criteria. The batch tests were then performed again, and the results were captured from both manufacturers. The results of this second set of batch tests are shown in Fig. 22 and Fig. 23.

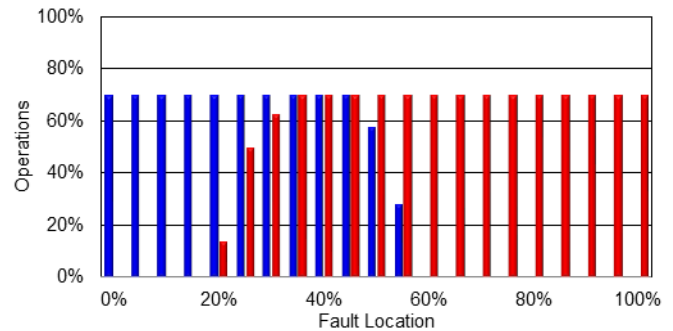


Fig. 22. Manufacturer A Zone 1 operations

With the reduced reach, the relays no longer transiently asserted Zone 1 at 85 to 90 percent of the line.

For Manufacturer B, the results shown in Fig. 23 are surprising given that only phase distance elements were used. For the first 10 percent of the line, the phase distance elements asserted for SLG faults, which was not an expected operation.

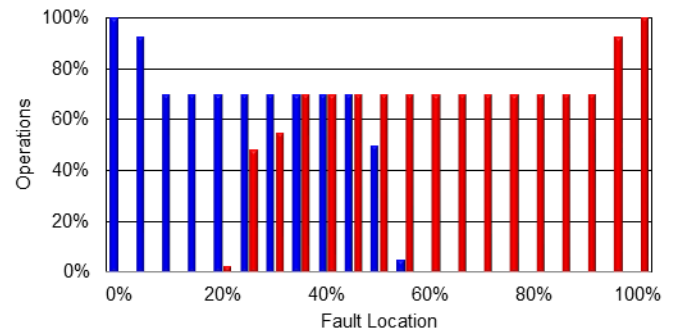


Fig. 23. Manufacturer B Zone 1 operations

Analyzing these results revealed that for this manufacturer and this firmware version, if the fault current magnitude was sufficiently high and the voltage was sufficiently low, the SLG fault would be pushed into the same quadrant as a phase-to-phase fault, and the phase distance elements would operate. In this application, neither the dependability nor the reliability of the relay was impacted; therefore, no changes were made.

2) *Overcurrent Elements*

Fig. 24 and Fig. 25 show the results of the batch tests performed to evaluate the performance of the instantaneous overcurrent elements. The overcurrent elements were expected to operate for no more than 60 percent of the applied faults because the elements only respond to faults involving ground.

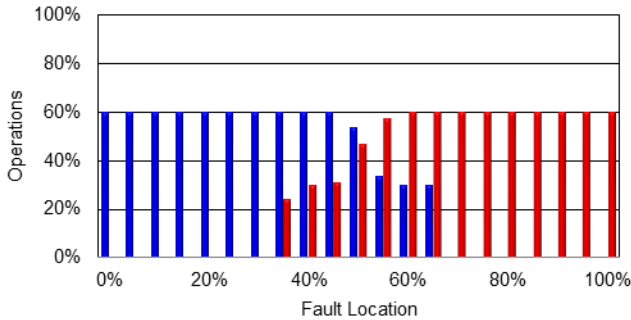


Fig. 24. Manufacturer A ground instantaneous overcurrent elements

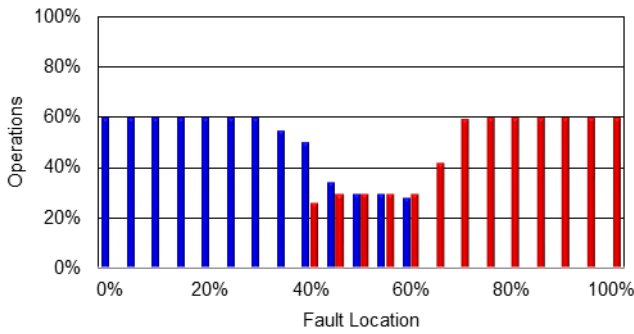


Fig. 25. Manufacturer B ground instantaneous overcurrent elements

No significant findings were discovered as a result of testing these elements. These results validated that the ground overcurrent was operating as expected.

3) *Relay Trip Times*

Relay trip times attained from the batch tests were recorded and plotted for the faults along the line. The results from Manufacturers A and B are shown in Fig. 26, Fig. 27, and Fig. 28. In these figures, blue and red indicate operating times for the Vincent and Mira Loma terminals, respectively. The communications channels for these devices were connected directly back to back with no channel impairment devices.

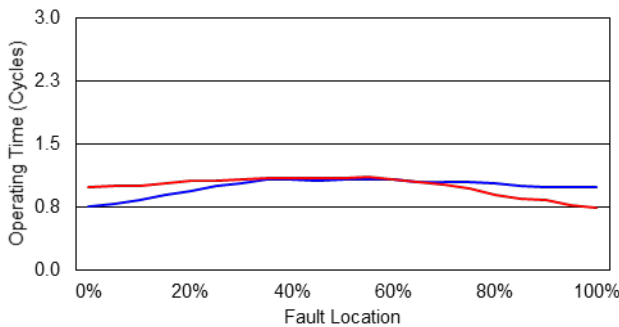


Fig. 26. Manufacturer A distance relay average trip times

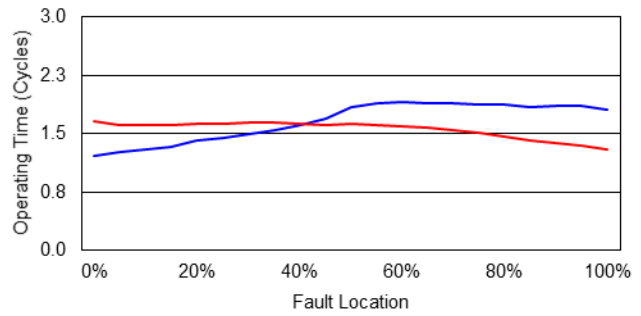


Fig. 27. Manufacturer B distance relay average trip times

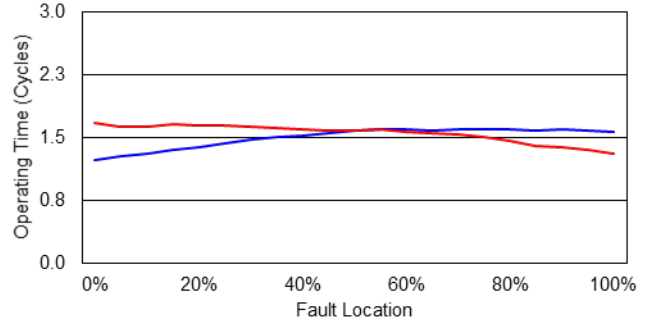


Fig. 28. Manufacturer B current differential relay average trip times

VI. FAULT LOCATING

Using real-time digital simulation, the impedance-based fault locators from both manufacturers were tested for SLG and three-lines-to-ground (3LG) faults in 5-percent increments along the line. Results from the Vincent terminal were recorded. Testing the Mira Loma terminal produced similar results (not shown).

A. *Impedance-Based Testing*

The results for the impedance-based test method at the Vincent terminal are shown in Fig. 29 through Fig. 32.

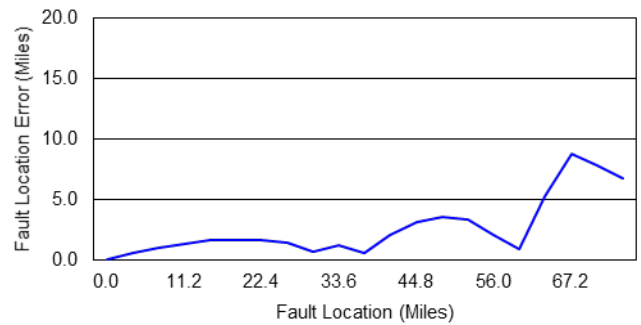


Fig. 29. Manufacturer A SLG impedance-based fault locator

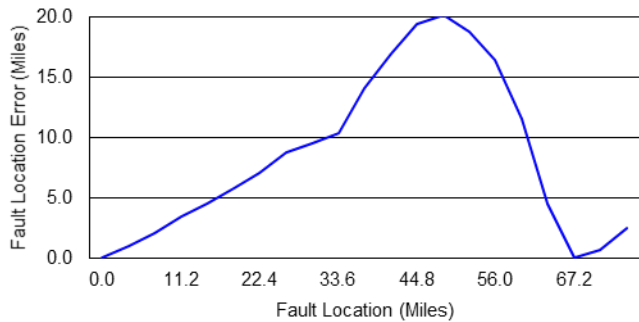


Fig. 30. Manufacturer A 3LG impedance-based fault locator

For Manufacturer A, the SLG fault locator had measurement errors up to 9 miles and the 3LG had measurement errors up to 20 miles.

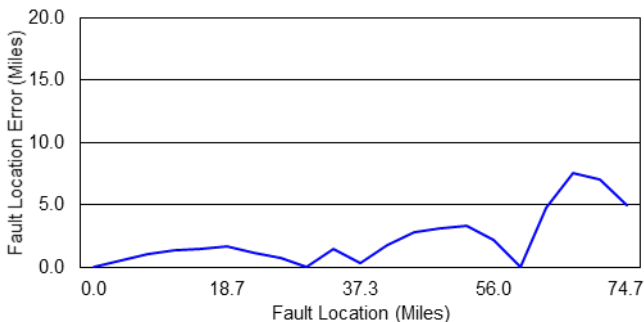


Fig. 31. Manufacturer B SLG impedance-based fault locator

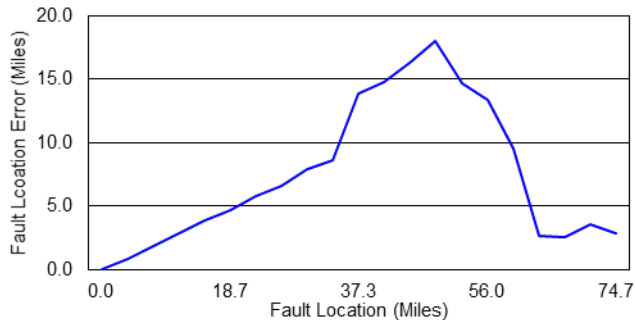


Fig. 32. Manufacturer B 3LG impedance-based fault locator

For Manufacturer B, the SLG fault locator had measurement errors up to 8 miles and the 3LG had measurement errors up to 18 miles.

Both manufacturers experienced similar errors in the accuracy of their impedance-based fault locators. These errors were mainly due to the split-phase section of the line, which affects fault locators similarly to distance elements.

### B. TW Testing, Theory, and Application

We explored TW fault locating to evaluate its functionality on this type of line composition using the line modeled in the real-time digital simulator. However, instead of performing the typical closed-loop testing in real time using a 50-microsecond time step, the real-time digital simulator was placed in a non-real-time mode and run at a time step of 320 nanoseconds. This allowed highly sampled COMTRADE files from the real-time digital simulator to be generated and

played back into the fault locating relays using time-aligned high-fidelity equipment.

Power system disturbances launch TWs, which can be detected by relays with TW detection capability [10] [11]. In typical line applications, the line is generally homogeneous (i.e., the line remains a similar construction throughout), which leads to a constant propagation velocity for the line. The Vincent-Mira Loma transmission line is classified as a composite line because the conductor type and tower configurations are not homogenous. The TW propagation velocity does not remain constant throughout composite lines. To accurately locate faults, a composite-line traveling-wave fault location (TWFL) algorithm is used. In order to accurately implement this algorithm, the TW propagation velocities and lengths of the four sections must be known.

Two methods exist for determining the section TW propagation velocities. Method 1 is based on derivations using tower geometries and conductor compositions. Method 2 uses line energization and back calculations.

Method 2 was chosen because the line was already modeled in an Electromagnetic Transients Program (EMTP). We simulated energization of the line from the Vincent terminal to generate and record the TWs necessary to calculate the separate section propagation velocities.

The following steps were performed to determine and validate the section velocities for facilitating accurate composite-line TWFL.

#### 1) Theory Explained

Use the following steps to perform section velocity calculations:

1. Build the line in EMTP using given conductor information and tower geometries.
2. Energize the line and record the sending terminal current waveforms.
3. Play sending terminal current signals into the relay using time-aligned, high-fidelity equipment. The relay records the event and produces a TW COMTRADE file.
4. Analyze the TW COMTRADE file to calculate the section velocities using a Bewley lattice diagram (Fig. 33).
  - a. Estimate the line junction reflection TW arrival times based on the section length and estimated section TW velocity range.
    - i.  $t_0$ : Breaker closing timestamp.
    - ii.  $t_1 = t_0 + (2 \cdot LL_1)/V_1$ : TW arrives from Line Junction 1–2. Multiply by 2 because the TW travels twice the length of Section 1.
    - iii.  $t_2 = t_0 + (2 \cdot LL_1)/V_1 + (2 \cdot LL_2)/V_2$ : TW arrives from Line Junction 2–3.
    - iv.  $t_3 = t_0 + (2 \cdot LL_1)/V_1 + (2 \cdot LL_2)/V_2 + (2 \cdot LL_3)/V_3$ : TW arrives from Line Junction 3–4.
    - v.  $t_4 = t_0 + (2 \cdot LL_1)/V_1 + (2 \cdot LL_2)/V_2 + (2 \cdot LL_3)/V_3 + (2 \cdot LL_4)/V_4$ : TW arrives from remote terminal.

- b. Match the TW arrival timestamps to their corresponding line junction.  
 c. Calculate the section velocities from the TW arrival timestamp information (13) through (16).

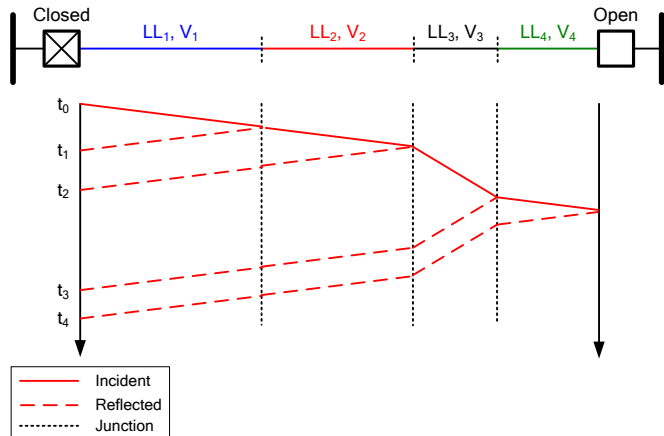


Fig. 33. Bewley lattice diagram showing expected TW arrivals.

The following section velocity calculations are based on the given TW arrival timestamps (in per unit of speed of light):

$$c = \text{speed of light} = \frac{186,000 \text{ miles}}{\text{second}} \quad (12)$$

$$V_1 = \frac{(2 \cdot LL_1)}{(c \cdot (t_1 - t_0))} \quad (13)$$

$$V_2 = \frac{(2 \cdot LL_2)}{(c \cdot (t_{12} - t_{21}))} \quad (14)$$

where:

$$t_{12} \text{ equals } t_1 - (LL_1/V_1)$$

$$t_{21} \text{ equals } t_2 - (LL_1/V_1)$$

$$V_3 = \frac{(2 \cdot LL_3)}{(c \cdot (t_{23} - t_{32}))} \quad (15)$$

where:

$$t_{23} \text{ equals } t_2 - (LL_1/V_1) - (LL_2/V_2)$$

$$t_{32} \text{ equals } t_3 - (LL_1/V_1) - (LL_2/V_2)$$

$$V_4 = \frac{(2 \cdot LL_4)}{(c \cdot (t_{34} - t_{43}))} \quad (16)$$

where:

$$t_{34} \text{ equals } t_3 - (LL_1/V_1) - (LL_2/V_2) - (LL_3/V_3)$$

$$t_{43} \text{ equals } t_4 - (LL_1/V_1) - (LL_2/V_2) - (LL_3/V_3)$$

## 2) Theory Applied

We played the EMTP files that generated secondary currents from the energization into the fault locating relay to record the response of the relay to the event. Fig. 34 shows the first cycle, where the black line is A-phase, the red line is B-phase, and the blue line is C-phase.

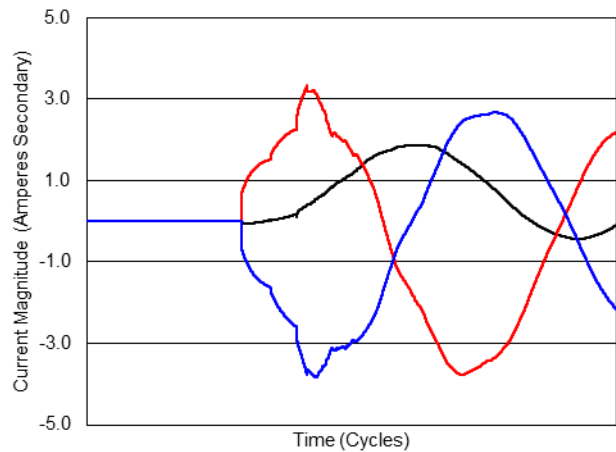


Fig. 34. Secondary currents injected into the relay

The relay TW fault locator captures the event and uses a high-pass filter to extract the TWs (Fig. 35). The TW event recorded captures the first half cycle of the currents shown in Fig. 34.

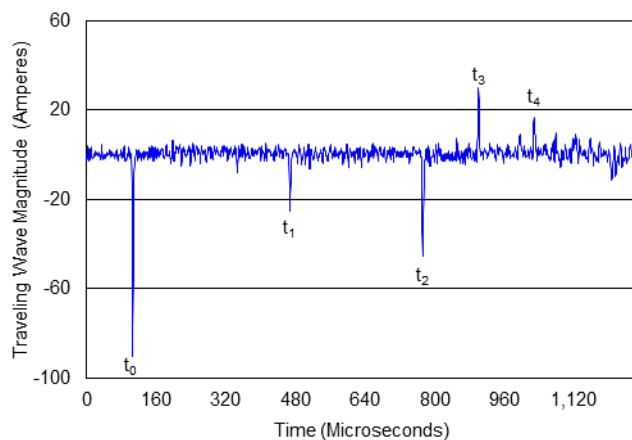


Fig. 35. Relay TW record

Using the TW COMTRADE files, timestamps are assigned to their corresponding line junctions. The first TW generated is from the breaker closing. We can anticipate when to expect the TWs from each line junction based on the known lengths and estimated section velocities ( $c$  for overhead and  $0.5 \cdot c$  for underground).

Table II lists the estimated and true arrival times of the TWs identified in Fig. 35.

TABLE II  
ESTIMATED AND TRUE TW ARRIVAL TIMES

Location	Estimated TW Arrival Time	True TW Arrival Time
Breaker close	$t_0 = 0.0001062 \text{ s}$	$t_0 = 0.0001032 \text{ s}$
Line Junction 1–2	$t_{1\_est} = 0.0004670 \text{ s}$	$t_1 = 0.0004646 \text{ s}$
Line Junction 2–3	$t_{2\_est} = 0.0007720 \text{ s}$	$t_2 = 0.0007699 \text{ s}$
Line Junction 3–4	$t_{3\_est} = 0.0008575 \text{ s}$	$t_3 = 0.0008966 \text{ s}$
Remote terminal	$t_{4\_est} = 0.0009507 \text{ s}$	$t_4 = 0.0009907 \text{ s}$

Once we have identified the timestamps belonging to the line junction reflections, we can use (12) through (16) to calculate the section TW propagation velocities:

$$V_1 = 0.9990$$

$$V_2 = 0.9991$$

$$V_3 = 0.3373$$

$$V_4 = 0.9904$$

### 3) Accuracy Results

Once the section velocities were identified, we generated the faults and validated the accuracy of the composite line TWFL algorithm. As before, faults were applied along the line in 5 percent increments, and the COMTRADE file for each fault was saved and subsequently played back into the relay. Fig. 36 shows the section velocity accuracy recorded by the relay where blue represents Section 1, red represents Section 2, black represents Section 3, and green represents Section 4.

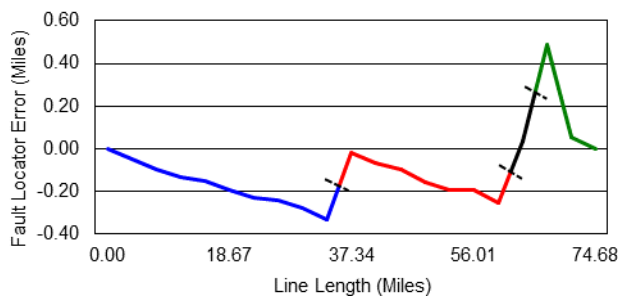


Fig. 36. Composite line TWFL accuracies

The composite line TWFL had an accuracy rating less than 0.50 miles from the theoretical location. This rating was within three tower spans (assuming a 900-foot tower span), yielding more accurate results than the impedance-based method.

## VII. CONCLUSION

SCE set forth to construct a new overhead transmission line to reduce congestion and improve reliability. During construction, the line was altered to incorporate an underground section. The protection package used was originally designed for overhead conductors; in retrospect, the protection package should have been reevaluated to include multiple line current differential relays. We used real-time digital simulation to validate the performance of protective relays, discover their limitations, and ascertain a proper course of action to mitigate the issues encountered. The Vincent-Mira Loma line composition led SCE to design and approve a new standard using a second line current differential scheme to be used on future lines.

This paper illustrates the following challenges:

- The impact of split-phase construction on the impedance calculated by a distance relay.
- The doubling of charging current drawn due to the parallel conductors as a result of split-phase construction.

- The significant voltage rise on the line caused by the excessive charging current drawn by the underground cables.
- The protection challenges associated with this line.

An exploration of TWFL allowed us to evaluate its functionality on this line composition and compare its accuracy to traditional impedance-based methods.

The line has not yet been energized to validate the work performed; nevertheless, this paper demonstrates a method to calculate the line impedance for different sections and reveals the significant errors in impedance-based fault locating methods caused by split-phase construction and underground cables.

## VIII. ACKNOWLEDGMENT

The authors gratefully acknowledge the contributions of Michael Thompson for his extensive work in real-time digital simulation.

## IX. REFERENCES

- [1] D. A. Tziouvaras, "Protection of High-Voltage AC Cables," proceedings of the 32nd Annual Western Protective Relay Conference, Spokane, WA, October 2005.
- [2] H.W. Dommel, "Overhead Line Parameters from Handbook Formulas and Computer Programs," *IEEE Transactions on Power Apparatus and Systems*, Vol. PAS-104, No. 2, February 1985, pp. 366–372.
- [3] E. O. Schweitzer, III, N. Fischer, and B. Kasztenny, "A Fresh Look at Limits to the Sensitivity of Line Protection," proceedings of the 37th Annual Western Protective Relay Conference, Spokane, WA, October 2010.
- [4] P. M. Anderson, *Analysis of Faulted Power Systems*. The Institute of Electrical and Electronic Engineers, Inc., NY, 1995.
- [5] D. A. Tziouvaras, H. J. Altuve, and F. Calero, "Protecting Mutually Coupled Transmission Lines: Challenges and Solutions," proceedings of the 40th Annual Western Protective Relay Conference, Spokane, WA, October 2013.
- [6] F. Plumtre, M. Nagpal, X. Chen, and M. Thompson, "Protection of EHV Transmission Lines with Series Compensation: BC Hydro's Lessons Learned," proceedings of the 62nd Annual Conference for Protective Relay Engineers, College Station, TX, March 2009.
- [7] G. Corpuz, K. Koellner, J. Bell, S. Rajan, A. Somani, and M. Thompson, "Series-Compensated Line Protection Challenges in the CREZ Region," proceedings of the 67th Annual Conference for Protective Relay Engineers, College Station, TX, March 2014.
- [8] C. R. Clarke, J. S. Park, C. Sanden, and T. Ninh, "Using a Real Time Digital Simulator to Test a Transmission Line with Asymmetrical Series Capacitors," proceedings of the 41st Annual Western Protective Relay Conference, Spokane, WA, October 2014.
- [9] E. O. Schweitzer, III and J. Roberts, "Distance Relay Element Design," proceedings of the 19th Annual Western Protective Relay Conference, Spokane, WA, October 1992.
- [10] E. O. Schweitzer, III, A. Guzmán, M. V. Mynam, V. Skendzic, B. Kasztenny, and S. Marx, "Locating Faults by the Traveling Waves They Launch," proceedings of the 40th Annual Western Protective Relay Conference, Spokane, WA, October 2013.
- [11] S. Marx, B. K. Johnson, A. Guzmán, V. Skendzic, and M. V. Mynam, "Traveling Wave Fault Location in Protective Relays: Design, Testing, and Results," proceedings of the 16th Annual Georgia Tech Fault and Disturbance Analysis Conference, Atlanta, GA, May 2013.

## X. BIOGRAPHIES

**Denis Bucco** is a protection supervisor in the engineering department of Southern California Edison. He received his BSEE from the Universidad de Carabobo in 2000 and his MSEE with honors from California State University, Los Angeles in 2003. He joined Southern California Edison as a protection engineer in 2003. He is a senior protection engineer with 13 years of experience working in the electric utility industry. He is a registered professional engineer in the state of California and a WPRC committee member.

**Curtis Sanden** is a senior protection engineer in the engineering department of Southern California Edison. He received his BSEE from California State Polytechnic University, Pomona in 1991. He joined Southern California Edison as a protection engineer in 1992 and has 24 years of experience working in the transmission and generation protection utility industry. He is a registered professional engineer in the state of California and a member of the WECC Relay Work Group.

**Arturo Torres** is a protection supervisor in the engineering department of Southern California Edison. He received his BSEE from California State University, Los Angeles in 1999. He joined Southern California Edison as a protection engineer in 1999. He is a senior protection engineer with 17 years of experience working in the electric utility industry.

**Edward Wong** is a protection supervisor in the engineering department of Southern California Edison. He received his BSEE from California State University, Los Angeles in 1991. He joined Southern California Edison as a protection engineer in 1991. He is a senior protection engineer with 25 years of experience working in the electric utility industry. He is a registered professional engineer in the state of California.

**Jordan Bell** received his BSEE from Washington State University and joined Schweitzer Engineering Laboratories, Inc. in 2008 as a protection engineer. He performs event report analysis, relay settings and relay coordination, fault studies, and model power system testing using a real-time digital simulator. He is a registered professional engineer in the state of Washington and a member of IEEE.

**Normann Fischer** received a Higher Diploma in Technology, with honors, from Technikon Witwatersrand, Johannesburg, South Africa, in 1988; a BSEE, with honors, from the University of Cape Town in 1993; a MSEE from the University of Idaho in 2005; and a PhD from the University of Idaho in 2014. He joined Eskom as a protection technician in 1984 and was a senior design engineer in the Eskom protection design department for three years. He then joined IST Energy as a senior design engineer in 1996. In 1999, Normann joined Schweitzer Engineering Laboratories, Inc., where he is currently a fellow engineer in the research and development division. He was a registered professional engineer in South Africa and a member of the South African Institute of Electrical Engineers. He is currently a senior member of IEEE and a member of ASEE.

**John Thompson** is an engineering intern with the Research and Development technology team at Schweitzer Engineering Laboratories, Inc. He received his BSEE at the University of Idaho in 2015 where he is currently pursuing his MA. He is a member of IEEE.